Journal of Qassim University for Science
2024, *Vol 3* (Issue 1), pp. 127-143
Received: 15 February 2024
Revised15 March 2024
Accepted: 15 April 2024

JQUS

Examination of the effect of Ti –doping on the crystallographic and transport characteristics of $La_{0.7}Sr_{0.25}Na_{0.05}Mn_{1-x}$ Ti_xO_3 (x = 0.0-0.2)

Rahma Ayed Brahem
Department of Physics, College of Science, Qassim University, Buraidah, 51452, Saudi Arabia
, E-mail R.brahem@qu.edu.sa

Abstract: In the present work, we investigated the effect of Ti-doping on the structural, electrical, and dielectric properties of $La_{0.7}Sr_{0.25}Na_{0.05}Mn_{1-x}$ Ti_xO_3(x =0.0-0.2). The investigated samples are elaborated via a conventional solid-state reaction route. To analyze the effects of the Ti doping on the physical properties of manganites,a coherent inquiry of the microstructural, structural, hopping transport, and dielectric relaxation behaviors in $La_{0.7}Sr_{0.25}Na_{0.05}Mn_{1-x}$ Ti_xO_3(x =0.0-0.2) was carried.This investigation is conducted to get a new comprehension of the impacts of the physical interactions between the titanium and manganese cations on the hopping conductivity and dielectric relaxation features of manganites. X-ray diffraction data and the Rietveld analysis displayed the occurrence of a rhombohedral phase with an$R\bar{3}c$space group. The substitution by Ti implies the increase of the lattice parameters from a=b=5.506 Å and c=13.360 Å for x=0.0 to a=b=5.531Å and c=13.416 Å for x=0.2. Using Scherer's equation, we found that the presence of Ti increases the crystallite size from 65.68 (4) nm for x=0.0 to 77.45 (2) nm for x=0.2. Via the Williamson-Hall (W-H) formula, it is found that the strain factor has decreased from 7.59 (2) $x10^{-4}$ for x=0.0 to 5.14 (3) $x10^{-4}$ for x=0.2.Using the SEM images, we found that the ceramics exhibit an average crystal size D_{MEB} that increases from 193 nm for $La_{0.7}Sr_{0.25}Na_{0.05}MnO_3$to 230 nm for $La_{0.7}Sr_{0.25}Na_{0.05}Mn_{0.8}Ti_{0.2}O_3$. Using the complex impedance and modulus studies, at room temperature, the obtained results revealed the presence of relaxation processes that are ascribed to the main roles of combined grain(G)and grain boundary (GB)domains. The compound's dielectric responses are explicated based on the phenomenological theory of Koop's and via the model of Maxwell–Wagner. The very low loss values for both compounds make this material family a good candidate for future applications like capacitors. The electrical conductivity spectra are analyzed based on the power law of Jonscher. They confirm that the Ti element's substitution reduces the prepared system's electrical DC conductivity from σ_{dc}=5.23 (4) 10^{-5} $S.m^{-1}$ for x=0.0 to σ_{dc}=3.86 (3) 10^{-5} $S.m^{-1}$ for x=0.2.

.

Keywords: ***Doped Manganites$La_{0.70}Sr_{0.25}Na_{0.05}Mn_{1-x}Ti_xO_3$; Structural properties; Transport characteristics; Impedance; Dielectric properties***.

1. INTRODUCTION

Nowadays, several perovskite solid solutions have involved significant consideration from the condensed matter community due to their motivating physicochemical characteristics **[1-3]**. In the literature, the physical properties (electronic, optoelectronic, mechanical, and thermoelectric properties characteristics) that make those materials good candidates for spintronics and optoelectronics applications are investigated via theoretical models**[4-7]**.For the aforementioned material family, an applied magnetic-type field is commonly accompanied by the appearance of a spectacular resistivity transition from the insulator to the metallic behaviors. The previously mentioned transition is mainly coupled with a magnetic change from the paramagnetic to ferromagnetic phases. This behavior favors the occurrence of the colossal magnetoresistance effect that makes this material family a good candidate for various technological applications. Additionally, due to the multifunctional behaviors of the manganite structures, this material family can be employed to fabricate multilayer ceramic capacitors and must be integrated in-memory storage and optoelectronic devices **[1-3, 8, 9]**. The conducted investigation by various research groups has shown that the manganite oxides reveal a strong correlation between orbital, charge carriers, spin orientations, and phonons

degrees of freedom. At low temperatures, ground states of manganite solid solutions are confirmed by the strong competition among localization tendency (interactions between eg electrons and Jahn–Teller (JT) distortion) and delocalization tendency of eg electrons. For the mixed valence manganites, the delocalization of electrons eg usually establishes the ferromagnetic behavior that is supported by the exchanges of charges between Mn^{3+} and Mn^{4+} cations via the oxygen (Zener's double-exchange effects) **[10, 11]**. In this context, the magneto-transport properties of the mixed valence manganite compounds can be mainly linked to the double exchange interactions that are controlled by the e_g electron's motion between the Mn cations **[12]**. In modern electronic technologies, $La_{1-x}Sr_xMnO_3$ (LSMO) system is widely employed in the field of the fabrication of solid oxide fuel cells (as a cathode) **[13-15]**. In this context, it has been confirmed that this material system is mentioned by the involvement of some tunneling/hopping motion mechanisms to the electrical transport motion of the charge carriers. As researcher groups have reported, the microstructure, which consists of "G" and "GB" effects, is the main factor determining the electrical and dielectric properties of compounds, as reported. According to V. Uskokovic et al. **[16]**, the LSMO perovskites are good applicant candidates in the biomedicine field (hyperthermia treatment). In this context, it has been confirmed that this structure reveals the need to distinguish healthy cells from malignant cells that are more vulnerable to temperature increase. Therefore, the LSMO system and its derivate can be employed in the cancer treatment domain. Besides, the above-mentioned structure reveals a motivating electro-conductivity that is associated with the ionic conduction related to the backbones of the conductor ions to produce raised-efficient cathodes. According to previous studies, it has been reported that the ferromagnetic state and charge-ordering/orbital-ordering are notably dependent on the cationic disorder effects (cation size mismatch) and the Mn-cation doping level **[17]**. Most of the available kinds of literature display that varying the Mn charges concentration touches strongly the fraction Mn^{3+}/Mn^{4+} that controls in turn the bond length and/or average Mn–O–Mn bond angle **[18]**. Likewise, the substitution at the manganese site cruelly hampers the DE network between the Mn cations that happens via the intermediate the oxygen anion that controls the density of the eg electron. This behavior influences strongly the electrical transport, the dielectric performance, and the magnetic characteristics of the manganite structures **[19]**. Especially, the presence of Ti in manganite solid solutions usually destroys the FM metallic states and persuades the occurrence of a cluster glass or a spin glass insulating state in the materials **[20]**. In the present research, we have elaborated $La_{0.7}Sr_{0.25}Na_{0.05}Mn_{(1-x)}Ti_xO_3$ to gain a piece of information about the impact of the Ti dopant at the Mn-site on the electrical and dielectric properties of the manganite compounds. According to previous conducted works, it has been confirmed that the Ti as a dopant element is mostly motivating as the cationic radius of the Mn^{4+} (0.530 A˚) is inferior as compared to the cationic radius of the Ti^{4+}cation (0.605 A˚) **[21]**. Nevertheless, the radius of Ti^{4+} is slightly lesser than the Mn^{3+} cation radius (0.645 A˚). Therefore, the substitution with the non-magnetic Ti cations removes the Mn^{4+} from the Zener double exchange interaction. This induces the occurrence of larger lattice strains in the material. The substation by Ti could likewise induce lattice distortions that expressively allow the impact of the lattice distortions variations on the displacement of the electron charges, the dielectric relaxations, and the magnetic performances in the manganite materials groups **[22]**. In the same context, the non-magnetic Ti transition metal element is responsible for the occurrence of elevated dielectric constant in various ferroelectric structures such as $PbTiO_3$, $BaTiO_3$, and $SrTiO_3$ compounds and their derivate **[23, 24]**. For $La_{0.4}Ca_{0.6}Mn_{0.4}Ti_{0.6}O_3$, it has been confirmed that the presence of the Ti at the Mn site has permed the occurrence of an unusually elevated dielectric

constant of about 6980 at 1 kHz **[25]**. This can be attributed to the fact that the presence of the Ti element favors the formation of barrier layers that enhance the dielectric performance of the manganite ceramics **[26]**.

We fully documented the doping effects on the electrical/dielectric characteristics of $La_{0.7}Sr_{0.25}Na_{0.05}Mn_{1-x}Ti_xO_3$(x =0.0-0.2) solid solution system. This work is bound to explain the structural (lattice distortion), the motion of the charges (displacement of electrons), and dielectric features of $La_{0.7}Sr_{0.25}Na_{0.05}Mn_{1-x}Ti_xO_3$(x =0.0-0.2) and to evaluate the effect of Ti substitution on the manganite's materials performance. The main objective of the present investigation is to extract ideas about the electron's dynamic and the possible relaxation phenomena in the $La_{0.7}Sr_{0.25}Na_{0.05}Mn_{1-x}Ti_xO_3$($0 \leq x \leq 0.2$) materials at 300 K and over a large frequency range using impedance spectroscopy. The novelty of the present investigation focuses on the impact of the structural parameter variations on the dielectric properties of the manganites. Accordingly, we search to improve the dielectric performances of manganites to make those materials potential candidates to stock the energy (good capacitors).

2. EXPERIMENTAL DETAILS

The studied $La_{0.7}Sr_{0.25}Na_{0.05}Mn_{1-x}Ti_xO_3$ ($0 \leq x \leq 0.2$) system is prepared using a conventional solid-state reaction route. La_2O3, $SrCO_3$, MnO_2, TiO_2, and Na_2O_3 reagent-grade oxide powder that exhibit high purity (all Aldrich make 99.99%) are employed as the starting materials. Using a temperature temperature-controlled programmable muffle furnace, the investigated samples are calcined at a temperature of 1000 °C with intermediate grindings for 3 days to remove carbon present. The calcined $La_{0.7}Sr_{0.25}Na_{0.05}Mn_{1-x}Ti_xO_3$ ($0 \leq x \leq 0.2$) powder is pressed into circular pellets form under 8 t/cm2 (of about 2 mm thickness) via a hydraulic press and for 48 h at 1350 °C in the air with intermediate milling and repulsive to attain the final materials. Lastly, the obtained pellets are quenched to room temperature. This step is achieved to preserve the crystalline structure at the annealing temperature. The phase purity and the crystal structure for each investigated compound are branded from the investigation of the X-ray diffraction at a temperature of 300 K. This analysis is carried out via a Siemens D5000 X-ray diffractometer that exhibits a radiation Cuk_α($\lambda_{Cuk\alpha}$=1.54Å) and over the Bragg angle range between $10° \leq 2\theta \leq 100°$. To analyze the response of the dielectric variation and electrical features in the solid solutions, an Agilent 4294A impedance analyzer is employed to extract the measurements over a wide frequency range **[27]**.

3. RESULTS AND DISCUSSION

3.1.Effects of Ti-doping on structural properties

Figure 1 displays the patterns of the powders that undergo X-ray diffraction at room temperature and the zoom-in of the principal peaks of the $La_{0.7}Sr_{0.25}Na_{0.05}Mn_{1-x}Ti_xO_3$ceramics. For each elaborated ceramic, the presence of sharp peaks with elevated intensity confirms the high crystalline quality of the ceramics. In addition, the reported result confirms the phase purity of $La_{0.7}Sr_{0.25}Na_{0.05}Mn_{1-x}Ti_xO_3$ ceramics (formation of single-perovskite phase).

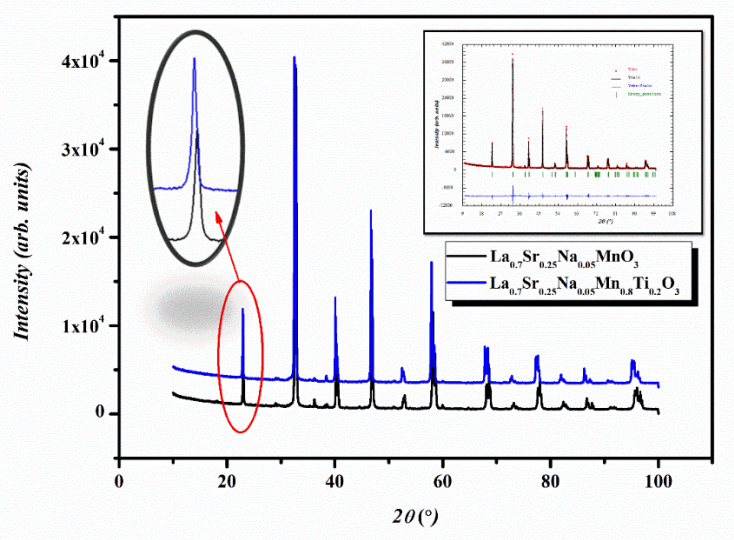

Figure 1: The $La_{0.7}Sr_{0.25}Na_{0.05}Mn_{1-x}Ti_xO_3$manganite's X-ray diffraction patterns. The inset exhibits the Ti-doping effect on the change in the main diffraction peak.

According to the results of the inset of **Figure 1**, we found that the main peak positions have shifted to an inferior 2θ angle due to the substitution of the system with the Ti^{4+} cations signifying the increase of the cell volume (V), which is directly linked to the lattice parameters (a, b, and c). A good correlation between our results and other reports can be remarked from the ref **[28]**. The increase in ''a'', ''b'', ''c'' and ''V'' parameters could be due to the difference between the ionic radii of the Ti^{4+} (r_{Ti}^{4+}= 0.605 Å) and the Mn^{4+} (r_{Mn}^{4+} = 0.53 Å) ions **[29]**. The XRD patterns were refined using the Rietveld method for studying the influence of the Ti-doping on the structural behaviors of the ceramics, the Rietveld refinement of the XRD patterns is reported to confirm that the studied system crystallizes in the distorted rhombohedral structure (space group: $R\bar{3}c$). For the undoped compound, the extracted lattice factor values are a=b=5.506 Å and c=13.360 Å. The substitution by the Ti cations is accompanied by the increases in the lattice parameter values that reach a=b=5.531Å and c=13.416 Å for the $La_{0.7}Sr_{0.25}Na_{0.05}Mn_{0.8}Ti_{0.2}O_3$compound. In the same context, the results resulted in a cell volume of 350.83 ($Å^3$) for the ceramic $La_{0.7}Sr_{0.25}Na_{0.05}MnO_3$and 355.56 ($Å^3$) for $La_{0.7}Sr_{0.25}Na_{0.05}Mn_{0.8}Ti_{0.2}O_3$. Using the XRD results, the size of crystallites and the strain of lattices values (β)for each studied sample are extracted by the following famous Williamson-Hall (W-H) expression **[30]**:

$$\beta = \beta_{size} + \beta_{strain} = \frac{k\lambda}{\beta_{hkl} cos\theta} + 4\varepsilon tan\theta \qquad (1)$$

The first and the second terms, which describe respectively the particle size and strain effects, reveal a Cauchy-like profile. The obtained line breadth for each compound can be defined as the sum of the aforementioned two contributions. The particle size is estimated using the following Scherer's equation **[31]**:

$$\beta_{size} = \frac{k\lambda}{\beta_{hkl} cos\theta} \qquad (2)$$

The factor *k* represents the grain shape factor, θ_{hkl}, and β_{hkl} are the diffraction angle (according to Bragg), and the broadening diffraction peaks according to the h, k, and l indexes, respectively. At half the peak maximum intensity, the β_{hkl} factor expressed in radians is computed for all the investigated solid solutions.

The broadening of Bragg's reflections (second term) is attributed to the micro strains effect. The determination of peak shift (β_{strain}) that is linked to the micro-strainεis determined using the Wilson formula **[32]**:

$$\beta_{strain} = 4\varepsilon tan\theta \qquad (3)$$

The micro-strain factors are dependent on numerous structural defects like the twin boundaries, dislocations, stacking faults, and intergrowths.

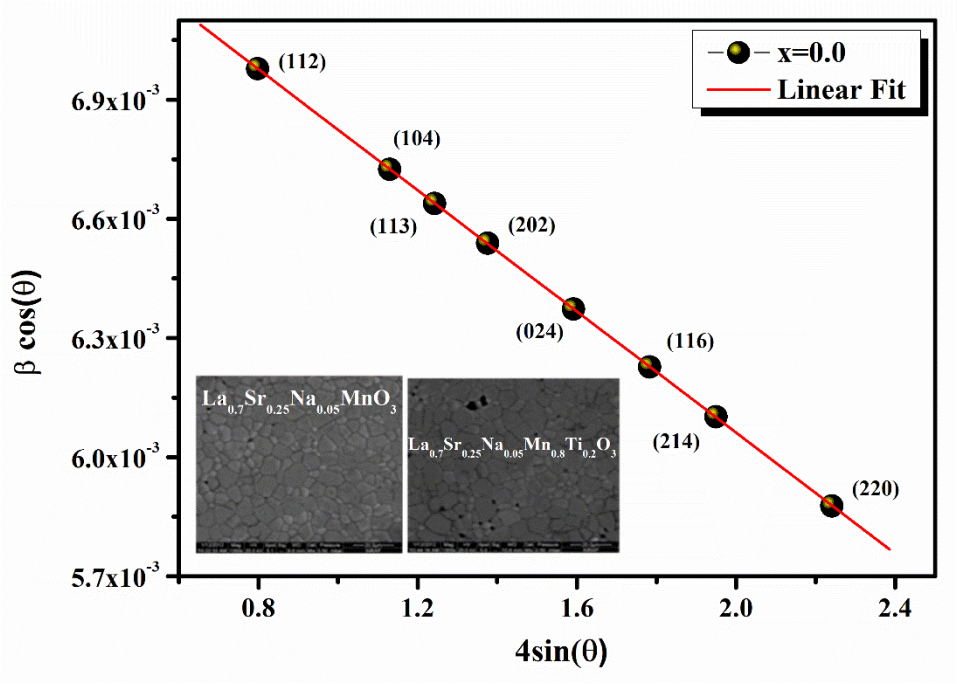

Figure 2: The plot of βcosθ as a function of 4sinθ of $La_{0.7}Sr_{0.25}Na_{0.05}Mn_{1-x}Ti_xO_3$ (x =0.0 and 0.2).

From the linear slope of $\beta\cos(\theta)$versus$4\varepsilon \sin(\theta)$, we have determined the lattice strain for each studied ceramic. Using the equation of W-H, the deduced strain parameter, from **Figure 2,** is illustrated in **Table 1.**

Samples	**Crystallite size (nm) Average grain size**			
	Williamson-Hall (W-H) Scherer's equation			**MEB**
	ε (x10^{-4})	β_{hkl}**(nm)**	D_{SC}**(nm)**	D_{MEB}**(nm)**
0.0	7.59 (2)	74.46 (3)	65.68 (4)	193 (1)
0.2	5.14 (3)	82.65 (1)	77.45 (2)	230 (2)

Table 1: X-ray diffraction and MEB parameters of the $La_{0.7}Sr_{0.25}Na_{0.05}Mn_{1-x}Ti_xO_3$ (x=0.0, 0.2) ceramics.

This parameter is found to decrease from ε=7.59 (2) 10^{-4} for the undoped sample to reach a value of ε = 5.14 (3) 10^{-4} for $La_{0.7}Sr_{0.25}Na_{0.05}Mn_{0.8}Ti_{0.2}O_3$. According to theW-H method and via Scherer's equation, the deduced average crystallite size (**Table 1**) is found to increase versus increasing the Ti content.

To extract an idea about the microstructural properties of the studied system and their dependence on the Ti content, Scanning Electron Microscopy (SEM) analysis was reported to control the average value of the particle size for each prepared ceramic. From the reported results in the inset of **Figure 2**, we found that the solid samples display a microstructure dense with big grains separated by remarkable resistive grain boundaries. Additionally, the substitution by the Ti increases the average grain size in the $La_{0.7}Sr_{0.25}Na_{0.05}Mn_{1-x}Ti_xO_3$system ($D_{MEB}$=230 nm for $La_{0.7}Sr_{0.25}Na_{0.05}Mn_{0.8}Ti_{0.2}O_3$compared to D_{MEB}=193 nm for$La_{0.7}Sr_{0.25}Na_{0.05}MnO_3$). For our case, the presence of Ti increases the grain size and favors the decreases in the density of the grains due to the chemical diffusion of isovalent ions to improve the compositional homogeneity of the compounds. As compared with the particle size that is obtained via the XRD results, the deduced grain size D_{MEB} calculated from the SEM images is much larger than D_{SC} demonstrating that each grain particle is composed of two or set crystallites.

3.2.Electrical investigation

3.2.1.Impedance formalism

To extrapolate information about the electrical responses in numerous materials compounds and to obtain an idea about the conduction and the relaxation mechanisms, the complex impedance investigation is mainly employed in the literature. This configuration gives precise information about the dependence of the charge displacement on the frequency and temperature increases. The resistive behavior and relaxation phenomena in the ceramic samples are examined using the real part (Z') and imaginary part (Z") of the complex impedance plots respectively **[33]**.

The relation between the frequency excitation and the complex impedance configuration (Z*)is defined below**.:**

$$Z^*(\omega) = Z'(\omega) + iZ''(\omega) \qquad (4)$$

Figure 3 illustrates the experimental Nyquist plots and the theoretical fits, at the ambient temperature for the studied compounds. Both Nyquist plots for the $La_{0.7}Sr_{0.25}Na_{0.05}Mn_{1-x}Ti_xO_3$ system exhibit one semi-circle arc, indicating the main importance of the "GB" influence on the dynamics of the charges of the prepared ceramics.

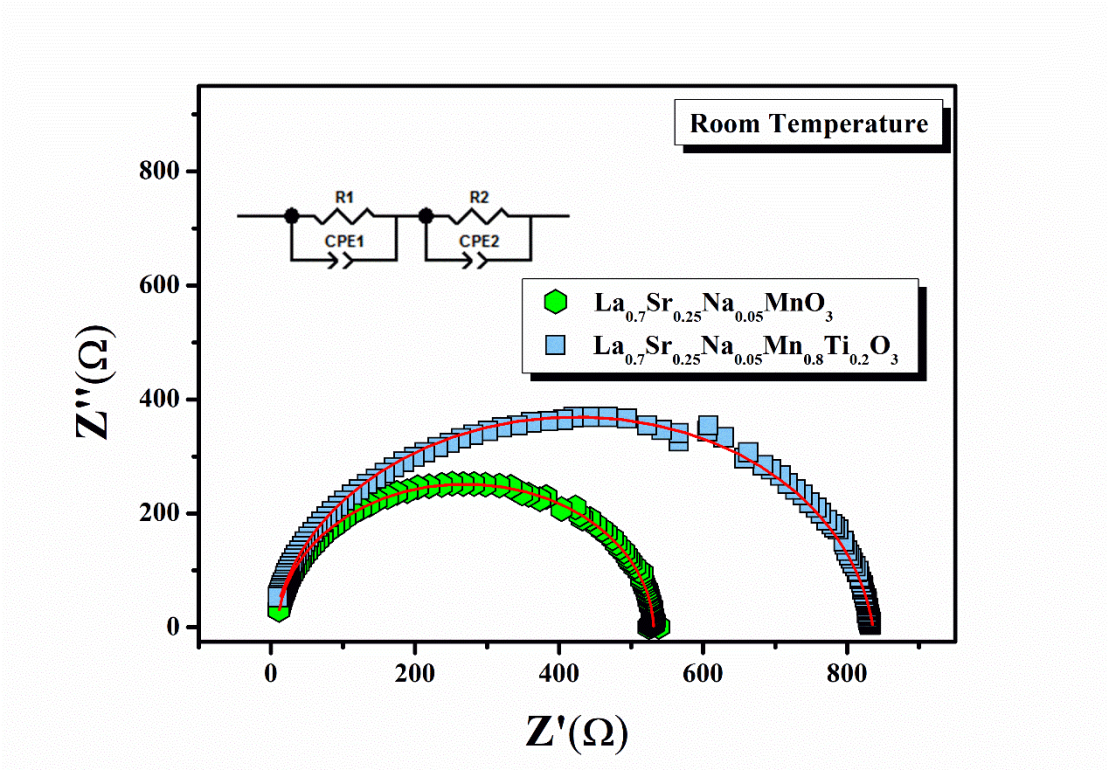

Figure 3: Nyquist plots for the $La_{0.7}Sr_{0.25}Na_{0.05}Mn_{1-x}Ti_xO_3$ (x =0.0 and 0.2) solid solutions. Inset: Equivalent electrical circuit for the $La_{0.7}Sr_{0.25}Na_{0.05}Mn_{1-x}Ti_xO_3$ compounds.

Instead of a centered semi-circle on the Z'-axis, the plotted semi-circles show a certain depression which confirms the non-Debye relaxation nature of compounds type perovskites **[34]**. In addition, this result indicates the distribution of a single relaxation time and evidence of the existence of polarization behaviors in the studied compounds **[35]**. In the literature, various factors like stress-strain phenomena, grain form, size and orientation, ''GB'', and atomic defect distribution are employed to explain the observed non-ideal behavior in ceramic systems **[36]**.

Both electrical and dielectric characteristics of solid solution ceramics are usually recognized as the combination of conducting "G" and resistive ''GB'' contribution **[37]**. As a result, we can assume that the resistance and the capacitance of the materials are both controlled by their microstructure. To determine the resistances and capacitances of "G" (R_g(the "G" resistance) and CPE_g (the "G" capacitance)) and "GB"(R_{gb}(the "GB" resistance) and $CPE_{gb}$the "GB" capacitance)), the obtained Nyquist plots of the $La_{0.7}Sr_{0.25}Na_{0.05}Mn_{1-x}Ti_xO_3$ system are fitted, at room temperature, using a Z-view software **[38]**. These kinds of representation are mainly employed to confirm the main contribution of the ''GB'' insulating zones to the conductivity of ceramics. The observed results in **Figure 3** confirm that the experimental data of the $La_{0.7}Sr_{0.25}Na_{0.05}Mn_{1-x}Ti_xO_3$compounds can be well modeled utilizing an equivalent circuit that contains R_x//CPE_x (x=g and x = gb) elements associated in series. The depicted circuit at the low-frequency region represents the electrical response from the ''GB'' domains, while the second circuit, at elevated frequencies, is attributed to the ''G'' response. For the studied ceramics, the deduced R_g, R_{gb}, CPE_g, and CPE_{gb} parameters are illustrated in **Table 2**.

Samples	$R_g(\Omega)$	R_{gb} (Ω)	$C_g(10^{-3}nF)$	$C_{gb}(10^{-3}nF)$
x=**0.0**	110	516	5.623	5.253
x= **0.2**	150	675	4.481	5.134

Table 2: Deduced electrical parameters using the Z-View software for both compounds.

For $La_{0.7}Sr_{0.25}Na_{0.05}Mn_{1-x}Ti_xO_3$ (x=0.0 and 0.2) samples, the R_{gb} resistances are significantly higher than the R_g resistances, which is the normal behavior of the grain boundaries that govern the conductivity in our materials**[39, 40].**

3.2.2.Conductivity analysis

To extract information about the AC conduction performance in materials, at 300 K, the evolution of the electrical conductivity is exposed in **Figure 4**.

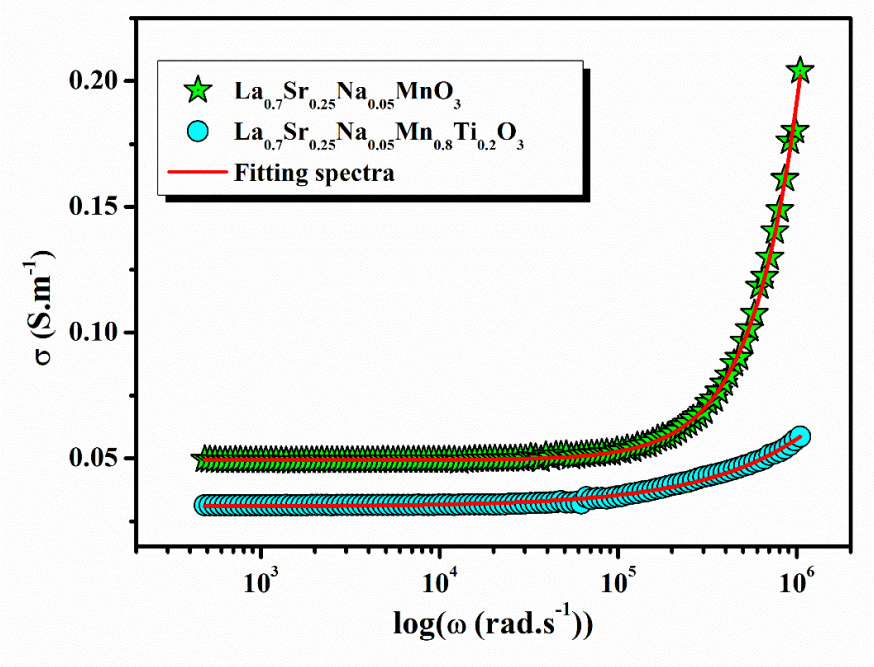

Figure 4: Frequency-dependent ac conductivity for $La_{0.7}Sr_{0.25}Na_{0.05}Mn_{1-x}Ti_xO_3$ (x=0.0 and x=0.2).

Both plotted spectra revealed a frequency-independent zone, below a critical frequency (hopping frequency), whichrepresents the direct current conductivity response of the compounds. At a relatively elevated frequency zone (the dispersive frequency side), the electrical conductivity variation obeys a power law like nature. At elevated frequencies, the conductivity increases is typically related to the hopping motions of charges **[41]**.Over the studied frequency region, the AC-conduction performances of the solid solutions are obtained by applying the Universal Dynamic Jonscher law (UDJL) **[42]**:

$$\sigma_{ac} = \sigma_{dc} + A\omega^n \qquad (5)$$

The factor ‘A’ is a temperature-dependent parameter. The exponent 'n' is a power exponent that measures the level of interaction between mobile ions and their surroundings. Using the UDJL, the fitted experimental data of the conductivity for the studied system are summarized in **Table 3**.

Samples	σ_{dc} (10^{-5} S.m^{-1})	A (10^{-9})	n
x=**0.0**	5.234	1.731	0.83
x= **0.2**	3.863	285 2	0.21

Table 3: Deduced electrical parameters using the Jonscher law for both compounds.

From our results, we found that the exponent "n'' value is found to decrease from n=0.83 for the $La_{0.7}Sr_{0.25}Na_{0.05}MnO_3$ compound to reach n=0.21 for $La_{0.7}Sr_{0.25}Na_{0.05}Mn_{0.8}Ti_{0.2}O_3$. This confirms that the substitution by the Ti element affects the level of interaction between mobile ions and their surroundings.We found that the exponent n is less than one for both compounds which is the normal behavior of manganite systems. The aforementioned conduction law is mainly employed to investigate the frequency dependence of the electrical conductivity for numerous manganite samples like the $La_{0.55}Ca_{0.45}Mn_{0.8}Nb_{0.2}O_3$**[43]**. According to the mentioned reference, the power law variation of the electrical conductivity is attributed to the activation of the correlated barrier hopping conduction process.

In the literature, the reported investigations in the field of the transport properties in the manganite compounds show that the dynamics of the charge carriers and the activation of the conduction mechanisms depend strongly on the microstructure that contains ''G'', ''Gb'', and pores **[44]**. For the manganite systems, the hopping motion of localized electric charge carriers across spatially lattice potentials that induce dipolar interactions mainly controls the electrical conductivity behavior of this material family **[45]**. From **Figure 4**, we found that the presence of diamagnetic Ti ions reduces the electrical conductivity of the system over the explored frequency domain. This result leads to enhancing the dielectric performances of the studied manganite system due to the connection between the dielectric breakdown phenomenon and the dielectric loss (that is related to the electrical conductivity variation). In this case, the decrease of the electrical conductivity versus increasing the Ti content level can make the $La_{0.7}Sr_{0.25}Na_{0.05}Mn_{1-x}Ti_xO_3$system a prominent candidate in the field of high-density capacitor systems **[46]**. Our findings are consistent with the literature **[47]**. In the present work, the reported results are probably attributed to the fact that the presence of the Ti^{4+} cations, which does not contain $3d$ electrons ((Ti^{4+} ([Ar] $3d^0 4s^0$))), will reduce the $3d$ electrons number that controls the motion of charges and the transport phenomena. Moreover, the substitution of the Mn^{4+} ions by the Ti^{4+} decreases the amount of Mn^{4+} holes destroys the Mn^{3+}- O-Mn^{4+} network portion, and introduces a cationic disorder collected with the change of an amount of the fraction bonds between Mn-O-Mn and Mn-O-Ti that decreases the conductivity of the Ti-doped manganite sample. Normally, the replacement of the Mn^{4+} by Ti^{4+} cations brings in a severe disorder to the ceramic compounds, which might favor the formation of Small Polaron charge carriers. Due to the difference in the cationic radius between the Mn and Ti elements, the substitution of the Mn element by the Ti one causes a variation in the cationic disorder, lattice parameters, bond angles, and distances of materials, which play crucial roles in both electrical and dielectric properties of the manganites, especially at low temperatures.

3.2.3.Electric modulus formalism

The modulus formalism ($M^*(\omega)$) is a convenient and imperative method for determining, analyzing, and interpreting the dynamics of the charge carriers' electrical conduction mechanisms, using conductivity relaxation

time and the carrier/ion hopping rate **[48]**. Accordingly, the abovementioned formalism can be used to investigate and describe the relaxation phenomena of the electric field when the electric displacement leftovers areconstant.
As compared with the complex impedance formalism, the modulus configuration provides information about the capacitive behavior of the material. The identification of the bulk ‘‘GB’’, which cannot be differentiated from complex impedance representations, can be achieved by using this representation to examine the inhomogeneous nature of ceramics.

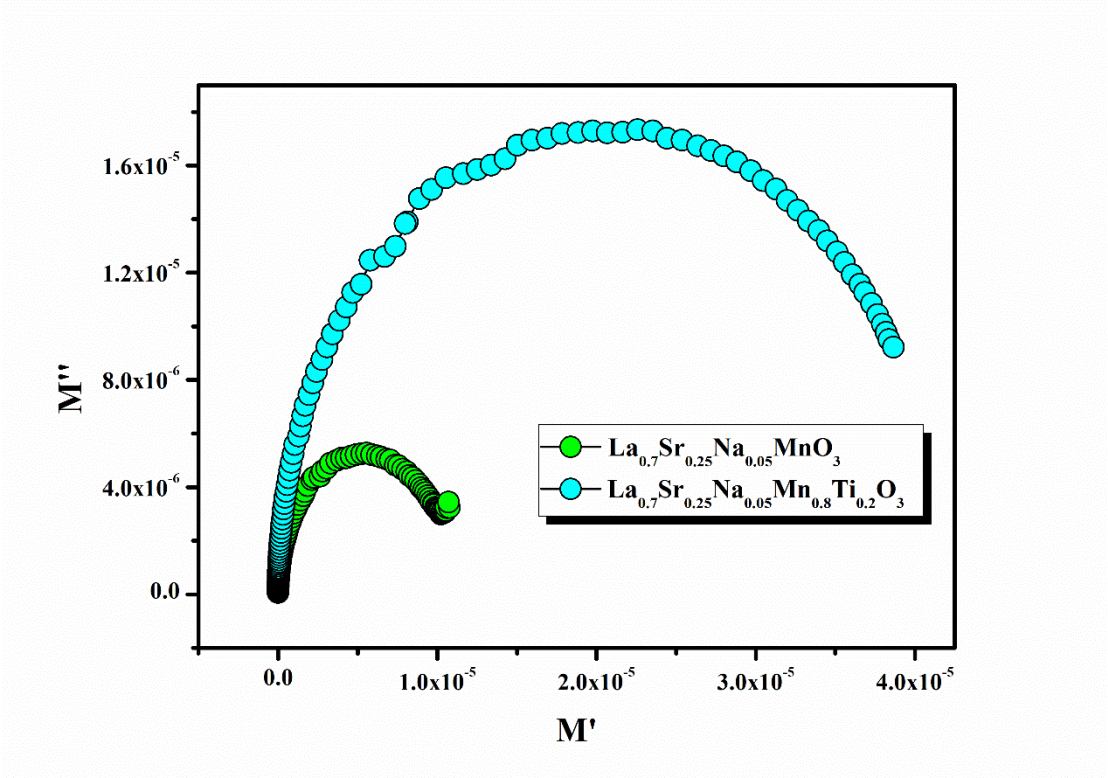

Figure 5: Complex modulus spectra for $La_{0.7}Sr_{0.25}Na_{0.05}Mn_{1-x}Ti_xO_3$ (x=0.0 and *x*=0.2).

Figure 5 illustrates the complex modulus spectra (M’’ vs M’) of the studied $La_{0.7}Sr_{0.25}Na_{0.05}Mn_{1-x}Ti_xO_3$(*x*=0.0 and 0.2) system. For each modulus Nyquist, The appearance of an arc approves the single phase of the studied ceramics. From the plotted results, the capacitive ‘‘G’’ effects can be determined at low frequencies, whereas the capacitive ‘‘GB’’ contribution can be noted at the high-frequency region. Both “GB” and “G” capacitances play an active role in the electrical properties of the studied $La_{0.7}Sr_{0.25}Na_{0.05}Mn_{1-x}Ti_xO_3$ (x=0.0 and 0.2) system. For our case, the substitution with the Ti^{4+} ions is accompanied by a growth in the plotted Nyquist radius confirming that the presence of Ti enhances the “G”capacitance of the studied ceramics.

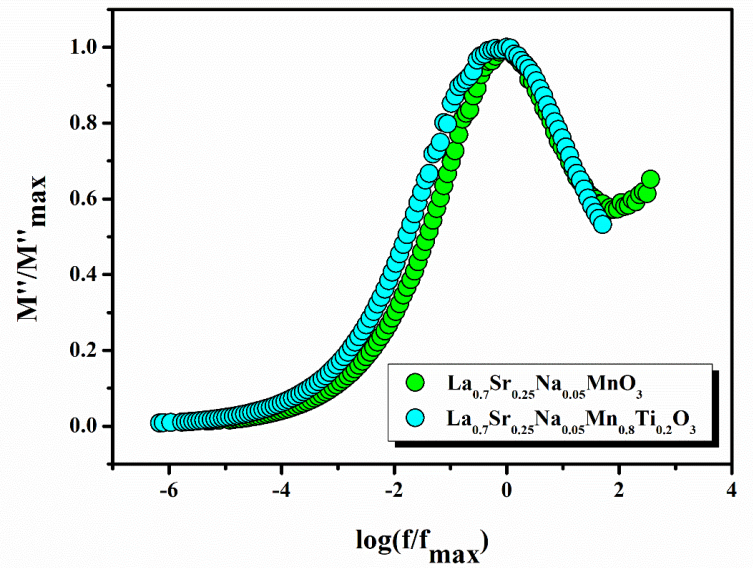

Figure 6: Correspondence between M''/M''$_{max}$ and log (f/f$_{max}$) for the perovskites $La_{0.7}Sr_{0.25}Na_{0.05}Mn_{1-x}Ti_xO_3$

Figure6 exhibits the evolution of M"/M"$_{max}$ vs. frequency, at T=300 K, of the $La_{0.7}Sr_{0.25}Na_{0.05}Mn_{1-x}Ti_xO_3$(x=0.0 and 0.2) ceramics. This kind of master-modulus representation can be employed to determine the parameter from the full width at demi M''/M''$_{Max}$ maximum. For the studied samples, the deduced value of β is found to decrease from 0.34 for $La_{0.7}Sr_{0.25}Na_{0.05}MnO_3$to reach 0.3 and $La_{0.7}Sr_{0.25}Na_{0.05}Mn_{0.8}Ti_{0.2}O_3$. The non-Debye relaxation nature of the solid ceramics is confirmed by the aforementioned obtained results. This suggests the existence of a poly-dispersive relaxation phenomenon in $La_{0.7}Sr_{0.25}Na_{0.05}Mn_{1-x}Ti_xO_3$(*x*=0.0 and 0.2).

The same phenomenon is recently reported for the case of the manganite $La_{0.55}Ca_{0.45}Mn_{0.8}Nb_{0.2}O_3$**[49]**. According to Moualhi *et al*, the non-Debye relaxation response of the compound is confirmed because the center of the semicircular pattern lies below the real axis. In addition, this phenomenon is confirmed by the fact that β is less than unity.

3.2.4.Dielectric properties

To get an idea about the consequence of the Ti-doping on the dissipated energy in a dielectric-prepared system, the variation of tanδ as a function of the frequency, at 300 K, is shown in **Figure7**.

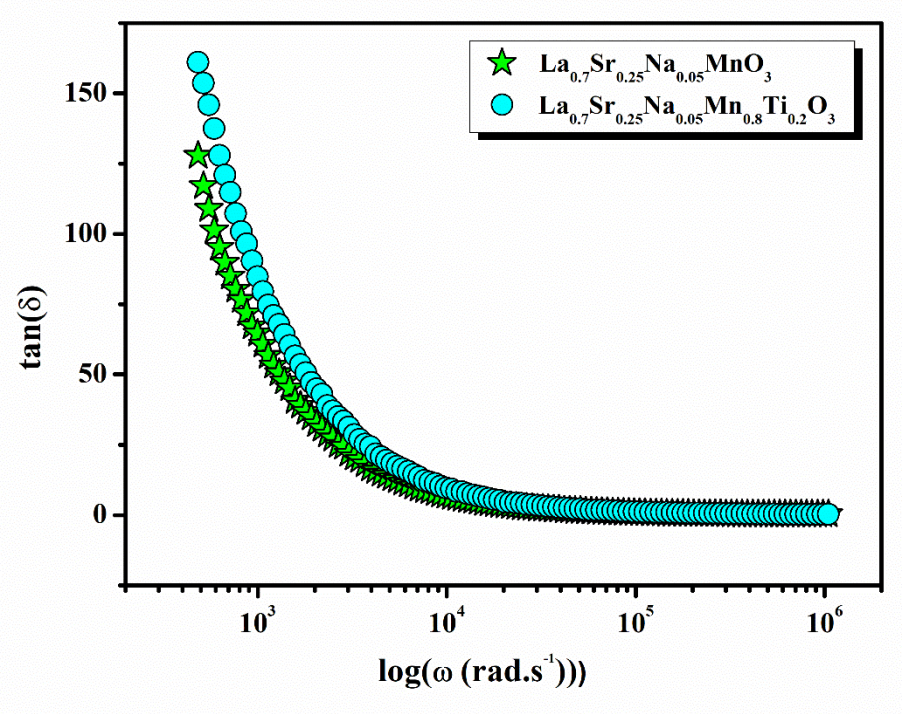

Figure 7: Frequency dependence of dielectric loss (tanδ) at room temperature for the studied compounds.

In the literature, the appearance of each tanδ is attributed to the existence of wall resonance. Dielectric losses are often observed when the effects of polarizations decrease with the applied alternating field. They result from impurities (oxygen deficiencies and defects in "GB") and imperfections in the crystal lattice, which depend in turn on the annealing temperature, and the substitution content **[50, 51]**. For the studied system, we observe from **Figure7** that the studied ceramics reveal a dispersion behavior in which (tanδ) is found to decrease and attain a minimum at elevated frequencies alike to the detected behavior for polar compounds **[52]**.

At low frequencies, the observed tan-like behavior can be described using Koop's theory by the Maxwell-Wagner interfacial polarization effects **[53]**. On this temperature side, the electrical resistivity is higher and the "GB" contribution is strong. In this case, more energy is required for the electron exchange between the Ti^{4+}, Mn^{4+},and Mn^{3+} ions. This leads to an intensification in the tanδ of the ceramics. The hopping probability increases continuously in the same way with the frequency rise, which corresponds to the increase in the conductivity due to the "G" effects, and therefore a small energy is essential for charge carrier motion between the adequate states. Thus, on the high-frequency side, the studied compounds exhibit a minimal loss tangent. Compared to $La_{0.7}Sr_{0.25}Na_{0.05}MnO_3$, the report indicates that $La_{0.7}Sr_{0.25}Na_{0.8}Ti_{0.2}O_3$ceramic reveals a small dielectric constant. Mainly, the charge displacement concerning the external field controls the hopping motion of the electrons among the localized states **[54, 55]**. For our case, the substitution by the Ti reduces the density of Mn^{4+}cations in the Mn site which could be principally accountable for the polarization of the space charges, and the hopping dynamic of the electrons. This decreases the polarization contribution in manganites and reduces the dielectric constant of the under-studied mixed valence samples.For our case, we have found that the substitution by the Ti element has decreased the strain value from 7.59 (2) $10^{-4}$for $La_{0.7}Sr_{0.25}Na_{0.05}MnO_3$ that reaches 5.14 (3) $10^{-4}La_{0.7}Sr_{0.25}Na_{0.05}Mn_{0.8}Ti_{0.2}O_3$. This can control mainly the dielectric properties of the studied system. The aforementioned properties are also controlled by other factors like the "G" and crystallite size and the lattice

parameters. Accordingly, variations in the dielectric performances of the sample could be attributed to the increase of the unit volume cell from V=350.83(1) $Å^3$ for $La_{0.7}Sr_{0.25}Na_{0.05}MnO_3$ to 355.56(1) $Å^3$for $La_{0.7}Sr_{0.25}Na_{0.05}Mn_{0.8}Ti_{0.2}O_3$.Moreover, we have found that the substitution by the Ti element has affects mainly the $\theta_{Mn/Ti\text{-}O\text{-}Mn/Ti}$angle that decreases from 166.67°from the parent compound to 165.87 165.13° for $La_{0.7}Sr_{0.25}Na_{0.05}Mn_{0.2}Ti_{0.2}O_3$, which controls mainly the hopping motions of the charge carriers and varies, in turn, the electrical and dielectric properties of the perovskite systems.

4. Conclusion

In summary, the investigated solid solutions are produced via the conventional solid-state reaction route.Influences of the presence of diamagnetic Ti cations in $La_{0.7}Sr_{0.25}Na_{0.05}Mn_{1-x}Ti_xO_3$ system are reported based on the microstructural, structural, electrical, and dielectric characterizations of the solid solution compounds. Therefore, experimental data and some theoretical models are presented in this work. The affined X-ray diffraction patterns approve the development of pure perovskite phases of a space group $R\bar{3}c$.According toScherer's equation, we have found that the Ti content increases followed by an increase incrystallite size from 65.68 (4) nm for x=0.0 to 77.45 (2) nm for x=0.2. Using the Williamson-Hall (W-H) formula, we found that the strain factor has decreased from 7.59 (2) $x10^{-4}$ for x=0.0 to 5.14 (3) $x10^{-4}$ for x=0.2.The impedance and the modulus analysis have shown the major effects ofboth conducting and resistive microstructure zones on the motion of electrons and dielectric relaxations. This kind of investigation has additionally long established that the substitution with the Ti lessens the Mn^{3+}–O–Mn^{4+} networks number and enhances the electrical resistance of the $La_{0.7}Sr_{0.25}Na_{0.05}Mn_{1-x}Ti_xO_3$ system. The Cole-Cole modulus analysis has revealed that both studied compounds exhibit a non-Debye relaxation process.

At 300 K, the conductivity spectra allure pursue a universal power law of Jonscher and approve the semiconductor nature of the $La_{0.7}Sr_{0.25}Na_{0.05}Mn_{1-x}Ti_xO_3$ system at high-frequency region. The tangent loss spectra are described in the limit of both the model of Maxwell–Wagner and the theory of Koop, which are responsible for electrical transport and the polarization effects in the perovskite systems.The electrical conductivity spectra confirm that the substitution by the Ti element reduces the electrical DC conductivity of the prepared system from σ_{dc}=5.23 (4) 10^{-5} $S.m^{-1}$ for x=0.0 to σ_{dc}=3.86 (3) 10^{-5} $S.m^{-1}$ for x=0.2. The studied systems are characterized by very low dielectric losses that make them potential candidates for future applications.

REFERENCES

[1] M. Smari, Y. Moualhi, Y. Tong, S. Mansour, H. Rahmouni, Magnetic effect and chemical distribution study of $LCMNO_3$ perovskite by photoelectron spectroscopy, Physica Scripta, 99.2 (2024) 025907.

[2] Y. Moualhi, M. Smari, H. Rahmouni, K. Khirouni Fundamental Behaviors, and Contributions of Hopping and Tunneling Mechanisms to the Transport Characteristics of the $La_{0.5}Ca_{0.5}MnO_3$ Phase Separated Perovskite, ACS Applied Electronic Materials 4.10 (2022) 4893-4902.

[3] Ch.-H. Lee, N. D. Orloff, T. Birol, Y. Zhu. Exploiting dimensionality and defect mitigation to create tunable microwave dielectrics. Nature 502 (2013) 532-536

[4] H. E M.M. Saad, Almeshal, A. Elhag, A. Alsobhi, B. O., D. P. Rai. Physical characteristics of crystal, magnetic, and electronic structures of Ce3+-based cubic perovskites CeTmO3 [Tm3+= Sc, Ti, V] investigated via the first-principles computational utilizing LDA, PBE-GGA and WC-GGA functionals. Indian Journal of Physics, 97(7) (2023) 2013-2031.

[5] H. E. M. M. Saad, Impact of 3d-transition metal [T= Sc, Ti, V, Cr, Mn, Fe, Co] on praseodymium perovskites $PrTO_3$: standard spin-polarized GGA and GGA+ U investigations, Bulletin of Materials Science, 45(2) (2022) 69.

[6] H. E.M. M. Saad, A. Elhag, Structural, magnetic, electronic and optical properties of cubic rare-earth vanadate perovskites $PrVO_3$ and $NdVO_3$: insights from GGA potentials,Indian Journal of Physics, (2021) 1-15.

[7] H. E. M. M. Saad, B. O Alsobhi, Consequences of Tuning Rare-Earth RE3+-Site and Exchange–Correlation Energy U on the Optoelectronic, Mechanical, and Thermoelectronic Properties of Cubic Manganite Perovskites $REMnO_3$ for Spintronics and Optoelectronics Applications, ACS omega, 7(32) (2022) 27903-27917.

[8] Y.Moualhi, H. Rahmouni, F. Bahri, Extremely consistent dielectric capacitors with excellent comprehensive dielectric permittivity characteristics using (Ba, Sr) (Ti, Zr) O3 lead-free ceramic-based relaxor ferroelectrics, Inorganic Chemistry Communications, 162 (2024) 112235.

[9]Y. Moualhi, H. Rahmouni, K. Khirouni, Usefulness of theoretical approaches and experiential conductivity measurements for understanding manganite-transport mechanisms, Results in Physics, 19 (2020) 103570.

[10] N. Rama, V. Sankaranarayanan, M. S. Ramachandra Rao,Role of double exchange interaction on the magnetic and electrical properties of ferromagnetic insulating manganiteJ. Appl. Phys. 99 (2006) 08Q315.

[11] S. J. Huang, J. D. Liu, Z. W. Pan, H. J. Zhang, B. J. Ye,Effect of intrinsic vacancies on the electromagnetic properties of half-doped $Sm_{0.5}Ca_{0.5}MnO_3$ manganites studied by positron annihilation, J. Appl. Phys. 134 (2023) 065104.

[12] J. Han, X. Yu, Sh. Jin, X. Guan, X. Gu, Y. Yan, K. Wu, L. Zhao, J. Jiang, J. Peng, Hongxi Liu, Xiang Liu, $Nd_{1-x}Sr_xMnO_3$ (x = 0.3): A perovskite manganite ceramic that exhibits PTC and NTC double properties, Ceramics International, 49 (2023) 4386-4392.

[13] Z. Xie, Z. Zou, X. Jiang, W. Zhang, Effects of A, B-site multiple ion co-doping on the structure, magnetic, magnetocaloric effect, and critical behavior of $La_{0.7x}Nd_{0.1}Sr_{0.2}K_xMn_{0.95}Ni_{0.05}O_3$ ceramics, Ceramics International 49 (2023) 32663-32678.

[14]A.T.Apostolov, I.N. Apostolova,J.M Wesselinowa, $La_{1-x}Sr_xMnO_3$ Nanoparticles for Magnetic Hyperthermia. Phys. Status Solidi B 255 (2018) 1700587.

[15]S. K. Chaluvadi, Z. Wang, L. M. C. de Araújo, P. Orgiani, V. Polewczyk, G. Vinai, O. Rousseau, V. Pierron, A. Pautrat, B. Domengès, D. G. Schlom, L. Méchin, Integration of epitaxial La2/3Sr1/3MnO3 thin films on silicon-on-sapphire substrate for MEMS applications, Applied Surface Science 579 (2022) 152095.

[16]V. Uskoković, M. Drofenik, Gold-embellished mixed-valence manganite as a smart, self-regulating magnetoplasmonic nanomaterial, Materials Chemistry and Physics, 271 (2021) 124870.

[17] Y. Moualhi, M. Smari, H. Rahmouni, K. Khirouni, E. Dhahri, Superlinear dependence of the conductivity, double/single Jonscher variations and the contribution of various conduction mechanisms in transport properties of $La_{0.5}Ca_{0.2}Ag_{0.3}MnO_3$ manganite, Journal of Alloys and Compounds, 898 (2022) 162866.

[18]X. Lang, H. Mo, X. Hu, H. Tian, Supercapacitor performance of perovskite $La_{1-x}Sr_xMnO_3$. Dalton Trans., 46 (2017) 13720-13730.

[19] P. Kaur, K. Singh, Structural, morphological and conducting properties of copper and nickel-substituted strontium manganite, Materials Today Communications, 35 (2023) 106056.

[20] D. Kumar, A. K. Singh, Structural and magnetic properties of Ti-substituted $La_{0.6}Ba_{0.4}Mn_{1-x}Ti_xO_{3-\delta}$ ($0.02 \leq x \leq 0.08$) perovskite manganites: Appearance of the Griffiths phase. Journal of Physics and Chemistry of Solids 176 (2023) 111253.

[21]A. Guedri, S. Mnefgui, S. Hcini, E.K. Hlil, A. Dhahri, B-site substitution impact on structural and magnetocaloric behavior of $La_{0.55}Pr_{0.1}Sr_{0.35}Mn_{1-x}Ti_xO_3$ manganites, Journal of Solid State Chemistry 297 (2021) 122046.
[22]L.H. Nguyen, N.T. Dang, N.V. Dang, L.V. Bau, P.H. Nam, L.T.H. Phong, D.H. Manh, P.T. Phong, Structural, magnetic, and electrical properties of Ti-doped $La_{0.7}Ba_{0.3}Mn_{1-x}Ti_xO_3$ ($0\leq x\leq 0.3$) ceramics, Journal of Alloys and Compounds 859 (2021) 157831.
[23]R.A. Evarestov, V.P Smirnov, D.E. Usvyat, Local properties of the electronic structure of cubic $SrTiO_3$, $BaTiO_3$ and $PbTiO_3$ crystals, analysed using Wannier-type atomic functions, Solid State Communications 127 (2003) 423-426.
[24]N. Bristowe, J. Varignon, D. Fontaine, P. Ghosez, Ferromagnetism induced by entangled charge and orbital orderings in ferroelectric titanate perovskites. Nat Commun 6 (2015) 6677.
[25] M. Li, A. Feteira, D. C. Sinclair, Origin of the high permittivity in $(La_{0.4}Ba_{0.4}Ca_{0.2})(Mn_{0.4}Ti_{0.6})O_3$ ceramics. J. Appl. Phys. 98, 084101 (2005).
[26]R. Hamdi, J. Khelifi, I. Walha, W Hzez, E. Dhahri,Structural and Dielectric Properties of $La_{0.5}Pr_{0.2}Ba_{0.3}Mn_{1-x}Ti_xO_3$ ($x = 0.0$ and 0.1) Manganite. J. Low Temp. Phys. 203 (2021) 158–179.
[27]Y. Moualhi, A. Mleiki, H. Rahmouni, K. Khirouni, Investigation of the dielectric response and the transport properties of samarium and strontium-based manganite, European Physical Journal Plus, 137 (2022) 406.
[28]G.D. Jadav, S.K. Chavda, P.V. Kanjariya, J.A. Bhalodia, Titanium effect on the structural, morphological and transport properties of $La_{0.7}Sr_{0.3}Mn_{1-x}Ti_xO_3$ ($x = 0.03$, 0.06 and 0.12), Materials Today: Proceedings 28 (2020) 432-439.
[29]S.Kh. Estemirova, V.Ya. Mitrofanov, S.A. Uporov, R.I. Gulyaeva, Effect of cation substitution on structural, magnetic and magnetocaloric properties of $(La_{0.7}Eu_{0.3})_{0.75}Sr_{0.25}Mn_{0.9}(Me)_{0.1}O_3$ (Me=Co, Ti), Journal of Magnetism and Magnetic Materials 502 (2020) 166593.
[30]P. M. Kibasomba, S. Dhlamini, M. Maaza, Ch.-Pu Liu, M. M. Rashad, Diaa A. Rayan, B. W. Mwakikunga, Strain and grain size of TiO_2 nanoparticles from TEM, Raman spectroscopy and XRD: The revisiting of the Williamson-Hall plot method, Results in Physics, 9 (2018) 628-635.
[31]P. Scherrer, Bestimmung der Grosse und innerenStruktur von KolloidteilchenmittelsRontgenstrahlen. NachGesWiss Gottingen, 2, (1918) 8-100.
[32] A.R. Stokes, A.J.C. Wilson, The diffraction of x rays by distorted crystal aggregates- I, Proc. Phys. Soc. 56 (1944) 174–181.
[33] L. Zhang, Y. Pu, M. Chen, Complex impedance spectroscopy for capacitive energy-storage ceramics: a review and prospects, Materials Today Chemistry. 28 (2023) 101353.
[34]M. Arora, V. Arora, Sh. Kaur, J. Kaur, S. Kumar, A. Singh, Evidence of non-Debye behavior of $Pb_{0.76}Sm_{0.24}Ti_{0.76}Fe_{0.24}O_3$ ceramics by complex impedance spectroscopy, Materials Today: Proceedings 80 (2023) 1079-1085.
[35]R. Das, R.N.P. Choudhary, Electrical and magnetic properties of double perovskite: $Y2CoMnO_6$, Ceramics International 47 (2021) 439-448.
[36]P. Nayak, A.K. Singh, Correlation between orthorhombic distortion with relaxation and Conduction mechanism of Gd^{3+} modified $SrBi_4Ti_4O_{15}$ ceramics, Ceramics International, 44 (2018) 22840-22849.
[37] N. S. Kumar, R. P. Suvarna, K. Ch.Babu Naidu, Grain and grain boundary conduction mechanism in sol-gel synthesized and microwave heated $Pb_{0.8-y}LayCo_{0.2}TiO_3$ ($y = 0.2$–0.8) nanofibers, Materials Chemistry and Physics, 223 (2019) 241-248.
[38] H. Salhi, Y. Moualhi, A.Mleiki, H. Rahmouni, K. Khirouni, Electrical and dielectric properties of the $La_{0.4}Bi_{0.3}Sr_{0.2}Ba_{0.1}MnO_3$ ceramic synthesized by sol–gel method, European Physical Journal Plus 138 (2023) 682.
[39]V. P. Kumar, V. Dayal, R. L. Hadimani, R. N. Bhowmik, D. C Jiles, Magnetic and electrical properties of Ti-substituted lanthanum bismuth manganites. J. Mater. Sci., 50 (2015)3562–3575.
[40]G. D. Jadav, P. V. Kanjariya, S. K. Chavda, and J. A. Bhalodia, Effect of Al and Ti substitution on the structural and magnetotransport properties of Lanthanum-Strontium manganite 1961 (2018) 1.
[41]A. Žužić, A. Ressler, A. Šantić, J. Macan, A. Gajović. The effect of synthesis method on oxygen nonstoichiometry and electrical conductivity of Sr-doped lanthanum manganites, Journal of Alloys and Compounds 907 (2022) 164456.
[42]A. K. Jonscher, New interpretation of dielectric loss peaks, Nature 253 (1975) 717-719.
[43]Y. Moualhi, M. Smari, H. Rahmouni, Understanding the charge carriers dynamics in the $La_{0.55}Ca_{0.45}Mn_{0.8}Nb_{0.2}O_3$ perovskite: scaling of electrical conductivity spectra, RSC Advances, 13 (2023) 30010.

[44]K. Snini, M. Akyol, M. Ellouze, L. El Mir, F. Ghribi, A. Ekicibil, Synthesis, structural characterization, electric and dielectric properties of $Pr_{0.67}Ba_{0.22}Sr_{0.11}Mn_{0.925}Ni_{0.075}O_3$ perovskite for thermal energy storage, Journal of Alloys and Compounds 874 (2021) 159866.
[45]H. Rahmouni, M. Smari, B. Cherif, E. Dhahri, K. Khirouni. Conduction mechanism, impedance spectroscopic investigation and dielectric behavior of $La_{0.5}Ca_{0.5-x}Ag_xMnO_3$ manganites with compositions below the concentration limit of silver solubility in perovskites ($0 \leq x \leq 0.2$). Dalton Trans., 44 (2015)10457-10466.
[46]Y. Wang, Z. Lv, L. Zhou, X. Chen, J. Chen, Y. Zhou, V. A. L. Roy and Su-Ting Han.Emerging perovskite materials for high density data storage and artificial synapses. J. Mater. Chem. C 6 (2018) 1600-1617.
[47]A. Anand, M. Manjuladevi, R. K. Veena, V. S. Veena, S. Sagar, A study on the thermopower and resistivity properties of Ti doped manganites $Gd_{0.7}Sr_{0.3}Mn_{1-x}Ti_xO_3$ (x = 0,0.1 and 0.15), Materials Today: Proceedings, 47 (2021)1829-1834.
[48]D. C. Sinclair, A. R. West, Impedance and modulus spectroscopy of semiconducting $BaTiO_3$ showing positive temperature coefficient of resistance, J. Appl. Phys. 66 (1989) 3850–3856
[49]Y. Moualhi, M. Smari, H. Nasri, H. Rahmouni, Combined transport and dielectric models and experimental characterization based on impedance spectroscopy for studying the microstructural and transport properties of electro-ceramic perovskites, Materials Today Communications, (2024) 108529.
[50]B. Yadav, K. K. Kar, M. K. Ghorai, D. Kumar, D.Yadav, Impact of defect migration on electrical and dielectric properties in molten salt synthesized $CaCu_3Ti_4O_{12}$ and customizing the properties by compositional engineering with Mg doping, Materials Chemistry and Physics 281 (2022) 125893.
[51]Y. Slimani, B. Unal, M.A. Almessiere, A. D. Korkmaz, S. E. Shirsath, G. Yasin, A.V. Trukhanov, A. Baykal, Investigation of structural and physical properties of Eu^{3+} ions substituted $Ni_{0.4}Cu_{0.2}Zn_{0.4}Fe_2O_4$ spinel ferrite nanoparticles prepared via sonochemical approach, Results in Physics,17 (2020) 103061.
[52]D. K.Mahato, T.P. Sinha, Dielectric, Impedance and Conduction Behavior of Double Perovskite Pr_2CuTiO_6 Ceramics. J. Electron. Mater., 46 (2017) 107–115.
[53]Z. Imran, M. A. Rafiq, M. M. Hasan, Charge carrier transport mechanisms in perovskite $CdTiO_3$ fibers AIP Advances, 4 (2014) 067137.
[54]M. B. Bechir, M. H. Dhaou, Study of Charge Transfer Mechanism and Dielectric Relaxation of $CsCuCl_3$ Perovskite Nanoparticles, Materials Research Bulletin 144 (2021) 111473.
[55]K. Moualhi, Y. Moualhi, M. Zouaoui, Investigation of conduction mechanisms and permittivity–conductivity correlation in a Gd-based perovskite structure, RSC Advances, 14, (2024) 4142.

الملخص باللغة العربية

تحليل تأثير إضافة التيتانيوم (Ti) على الخصائص البلورية والنقلية لمركب $La_{0.7}Sr_{0.25}Na_{0.05}Mn_{1-x}Ti_xO_3$ (x = 0.0-0.2)

رحمة عياد ابراهم

المملكة العربية السعودية، القصيم ،بريدة، جامعة القصيم ،كلية العلوم، قسم الفيزياء

قمنا بدراسة تأثير إضافة التيتانيوم على الخصائص الهيكلية والكهربائية والعازلة للمادة $La_{0.7}Sr_{0.25}Na_{0.05}Mn_{1-x}Ti_xO_3$ (x = 0.0-0.2) . حيث تم تحضير العينات المدروسة عبر طريقة تفاعل الحالة الصلبة التقليدية. لتحليل تأثير إضافة التيتانيوم على الخصائص الفيزيائية لمركبات المنجنيت، تم إجراء استقصاء متسق للسلوكيات الميكروهيكلية والهيكلية ونقل القفزات والاسترخاء العازل في مادة La0.7Sr0.25Na0.05Mn1-xTixO3 (x = 0.0-0.2). تم إجراء هذه الدراسة للحصول على فهم جديد لتأثيرات التفاعلات الفيزيائية بين أيونات التيتانيوم والمنجنيز على السلوك التوصيلي للقفزات وخصائص الاسترخاء العازلة لمركبات المنجنيت. أظهرت بيانات حيود الأشعة السينية وتحليل ريتفيلد حدوث مرحلة رومبوهيدرالية بمجموعة فضائية $R\bar{3}c$. يعني الاستبدال بواسطة التيتانيوم زيادة في معلمات الشبكة من a=b=5.506 Å و c=13.360 Å لـ x=0.0 إلى a=b=5.531 Å و c=13.416 Å لـ x=0.2. باستخدام معادلة شيرر، وجدنا أن وجود التيتانيوم يزيد من حجم البلورات من 65.68 (4) نانومتر لـ x=0.0 إلى 77.45 (2) نانومتر لـ x=0.2. من خلال صيغة ويليامسون-هول(Williamson-Hall) ، تم العثور على أن عامل الإجهاد قد انخفض من 7.59 (2) x10-4 لـ x=0.0 إلى 5.14 (3) x10-4 لـ x=0.2. باستخدام صور الإلكترون الضوئي الماسي(SEM) ، وجدنا أن الخزف يظهر حجم بلوري متوسط DMEB يزيد من 193 نانومتر لـ La0.7Sr0.25Na0.05MnO3 إلى 230 نانومتر لـ La0.7Sr0.25Na0.05Mn0.8Ti0.2O3. من خلال دراسات الانتشار المعقد والمودلس، في درجة حرارة الغرفة، أظهرت النتائج المحصل عليها وجود عمليات استرخاء يُنسب إلى الأدوار الرئيسية لمناطق الحبيبات المجتمعة (G) وحدود الحبيبات (GB). تم تفسير استجابات العازل للمركب بناءً على نظرية كوب وعبر نموذج ماكسويل-واجنر. قيم فقدان منخفضة جدًا لكلا المركبين تجعل هذه العائلة المادية مرشحة جيدة للتطبيقات المستقبلية مثل المكثفات. تم تحليل طيف التوصيل الكهربائي استنادًا إلى قانون السلطة لجونشر. يؤكدون أن استبدال عنصر التيتانيوم يقلل من توصيلية التيار المستمر الكهربائي للنظام المحضر من σdc=5.23 (4) 10-5 S.m-1 لـ x=0.0 إلى σdc=3.86 (3) 10-5 S.m-1 لـ x=0.2.

الكلمات المفتاحية: منجنيتات مشوبة بالتيتانيوم ($La_{0.7}Sr_{0.25}Na_{0.05}Mn_{1-x}Ti_xO_3$ (x = 0.0-0.2), الخصائص الهيكلية, الخصائص النقلية,المعاوقة,الخصائص العازلة.